Constraining safe and unsafe overshoots in saddle-node bifurcations

Elias Enache, Oleksandr Kozak, Nico Wunderling, Jürgen Vollmer

Originally published as
Enache, E., Kozak, O., Wunderling, N., Vollmer, J. (2025): Constraining safe and unsafe overshoots in saddle-node bifurcations. - Chaos, 35, 1, 013157.
https://doi.org/10.1063/5.0197940

Chaos
An Interdisciplinary Journal of Nonlinear Science

RESEARCH ARTICLE | JANUARY 27 2025

Constraining safe and unsafe overshoots in saddle-node bifurcations

Elias Enache ; Oleksandr Kozak ; Nico Wunderling ; Jürgen Vollmer

Chaos 35, 013157 (2025)
https://doi.org/10.1063/5.0197940

Constraining safe and unsafe overshoots in saddle-node bifurcations

Cite as: Chaos 35, 013157 (2025); doi: 10.1063/5.0197940
Submitted: 15 January 2024 · Accepted: 29 December 2024 ·
Published Online: 27 January 2025

Elias Enache,[1] Oleksandr Kozak,[1] Nico Wunderling,[2,3,4,a)] and Jürgen Vollmer[1,b)]

AFFILIATIONS

[1]Institute for Theoretical Physics, University of Leipzig, D-04081 Leipzig, Germany
[2]Center for Critical Computational Studies (C^{3}S), Goethe University, 60629 Frankfurt am Main, Germany
[3]Earth Resilience Science Unit, Potsdam Institute for Climate Impact Research (PIK), Member of the Leibniz Association, D-14437 Potsdam, Germany
[4]Stockholm Resilience Centre, Stockholm University, SE-106 91 Stockholm, Sweden

[a)]**Author to whom correspondence should be addressed:** nico.wunderling@pik-potsdam.de
[b)]juergen.vollmer@uni-leipzig.de

ABSTRACT

We consider a dynamical system undergoing a saddle-node bifurcation with an explicitly time-dependent parameter $p(t)$. The combined dynamics can be considered a dynamical system where p is a slowly evolving parameter. Here, we investigate settings where the parameter features an overshoot. It crosses the bifurcation threshold for some finite duration t_e and up to an amplitude R, before it returns to its initial value. We denote the overshoot as safe when the dynamical system returns to its initial state. Otherwise, one encounters runaway trajectories (tipping), and the overshoot is unsafe. For shallow overshoots (small R), safe and unsafe overshoots are discriminated by an inverse square-root border, $t_e \propto R^{-1/2}$, as reported in earlier literature. However, for larger overshoots, we here establish a crossover to another power law with an exponent that depends on the asymptotics of $p(t)$. For overshoots with a finite support, we find that $t_e \propto R^{-1}$, and we provide examples for overshoots with exponents in the range $[-1, -1/2]$. All results are substantiated by numerical simulations, and it is discussed how the analytic and numeric results pave the way toward improved risk assessments separating safe from unsafe overshoots in climate, ecology, and nonlinear dynamics.

Tipping points are critical thresholds in dynamical systems at which small perturbations may lead to a qualitative and possibly irreversible change of the dynamical system's state.[1–6] Often these tipping points are crossed only up to a certain amplitude R and for some finite duration t_e, before the parameters return to their sub-threshold values. In geology, this applies for heavy rainfalls inducing landslides.[7–9] In economy, this is a common scenario for bank stress tests.[10] In neural dynamics, it is a core idea in the criticality hypothesis modeling the brain computational properties.[11] In the Earth's climate system, the tipping points for melting the large ice sheets on Greenland or Antarctica may be crossed at least temporarily due to ongoing global warming.[12–14] In all cases, it is vital to identify the boundary between safe overshoots, where the system returns to its initial state without tipping, and unsafe overshoots, where tipping events are triggered. Earlier literature[15] reported an inverse square-root law as boundary between safe and unsafe overshoots. Here, we introduce a dimensionless overshoot amplitude H and duration T, and we establish that the scaling $T \sim H^{-1/2}$ applies for shallow overshoots $H \simeq 1$. For larger overshoot amplitudes $H \gtrsim 1$, there is a crossover to a steeper power-law decay with exponents in the range between $-1/2$ and -1. We provide upper bounds for parameter profiles that decay with different powers, and by numerical work, we show that these bounds are sharp. Hence, the safe region in parameter space is substantially smaller than expected, with severe consequences for the risks assessments of separating safe from unsafe overshoots.

I. INTRODUCTION

Tipping emerges when an asymptotic state of a dynamical system disappears in a saddle-node bifurcation.[3–5,16,17] We will characterize the state of the system by the scalar variable $x(t)$, and assume that its equilibrium state x_∞ changes continuously upon changing a

control parameter r for values $r < 0$. At $r = 0$, the dynamical system undergoes a saddle-node bifurcation where x_∞ fuses with an unstable fixed point: For $r < 0$, there is a region of initial conditions that converge toward x_∞, and for $r > 0$, these initial conditions will run away to a different attractor. Here, we are interested in situations where the control parameter is varied in time $r(t)$: For late and early times, it approaches $-R_d < 0$; at time $t = 0$, it takes its maximum value $R > 0$; and it takes positive values for a time interval of duration t_e. We denote this behavior as an overshoot of duration t_e and amplitude R. When the overshoot is sufficiently shallow and short, i.e., when R and t_e are both small, the system will return to its initial state. We denote this as a *safe overshoot*. An overshoot where the system runs away to another attractor will be denoted as an *unsafe overshoot*.

Overshoots have been discussed in the field of nonlinear systems and bifurcation theory over recent years.[12,15] The main question for general systems is whether we observe a return to the original state after the control parameter falls below the critical value again. This question may be relevant for various applications in finance, politics, or ecology.[4,18] Moreover, recently, overshoots received particular attention in climate science,[19–21] because there are several subsystems of the Earth that may exhibit threshold behavior.

Based on a multiple time scale analysis,[16,22] Ritchie *et al.*[15] established that the border separating safe and unsafe overshoots takes the form of a power law, $R\,t_e^2 = \text{const}$, provided that R is small, t_e is large, and that the overshoot takes the form of a parabola. This dependence is shown by the uppermost, black dotted line in Fig. 1. In the present paper, we extend this result to all values of R and arbitrary form of the overshoot (other lines in Fig. 1):

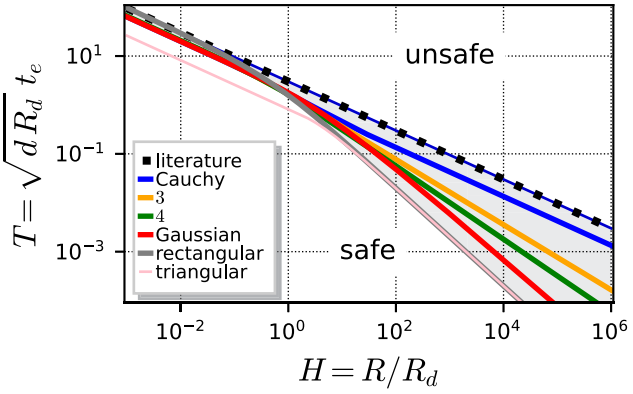

FIG. 1. The border dividing the parameter space spanned by the dimensionless overshoot amplitude H and overshoot duration T [both introduced in Eq. (7)] into a safe region (no tipping) and an unsafe region (tipping). The different lines refer to different shapes of the overshoot with the same amplitude and duration. The uppermost, dotted black line corresponds to the results from the literature[15] and follows a power law. Numerical results from the present article for an overshoot following a Gaussian shape are represented by the red solid line and those for distributions decaying to their asymptotic values with power laws with exponents 2 (Cauchy distribution), 3 and 4 by blue, orange, and green solid lines, respectively. The solid gray line provides the boundary for a discontinuous, piecewise-constant dependence of $r(t)$.

For $R \lesssim R_d$, we recover the power law suggested in the literature. Different shapes of $r(t)$ only slightly modify the prefactor of the power law.

For $R \gtrsim R_d$, the boundary changes qualitatively. It crosses over to a steeper power law with an exponent that depends on the asymptotic decay of $r(t)$ toward R_d. We determine the corresponding power and potential logarithmic corrections.

For triangular overshoots, we explicitly show that these results also apply when the overshoots are asymmetric and when they do not have a quadratic tip.

This paper is organized as follows. In Sec. II, we determine the boundary of the stable region for a piecewise-constant overshoot trajectories. Subsequently, we use this analytical result to establish upper and lower bounds for the boundaries of systems where the overshoots deviates from R_d only for a finite time (Sec. III A) and where they take a general unimodal shape (Sec. III B). In Sec. IV A, we discuss the bounds for overshoots with a Gaussian shape, as previously considered in the literature,[15] and Sec. IV B deals with overshoots with power-law tails. In the discussion (Sec. V), we revisit the earlier findings[15] and discuss the relevance of our findings for climate models. Key findings are summarized in Sec. VI.

II. SOLUTION FOR RECTANGULAR OVERSHOOTS

We consider a system described by a variable $x(t)$ with a dynamics close to a saddle-node bifurcation upon varying a parameter, r. Accordingly, the dynamics takes the form

$$\dot{x} = F(x;r) \simeq r\,(1 + 2\,a\,x) + b\,x^2 + f(x;r)\,, \tag{1}$$

where $f(x,r)$ comprises terms that are at least cubic in x. In general, a and b are continuous functions of r, i.e., for small r, we have $a \simeq a_0 + a_1\,r + \cdots$ and $b \simeq b_0 + b_1\,r + \cdots$ with $b_0 > 0$. Consequently, the dynamics has two fixed points x_- and x_+ that collide and undergo a saddle-node bifurcation at $x = 0$ when r traverses $r = 0$. This setting is illustrated in Fig. 2 where the solid blue (lowermost at $x = 0$) line shows $F(x;-R_d)$ for some value $r = -R_d < 0$, the solid gray line shows $F(x;0)$ that follows $b_0\,x^2$ for small x, and the solid red line (uppermost thick line at $x = 0$) shows $F(x;R)$ for some value $r = R > 0$, respectively.

In the present section, we explore if the dynamics return to the stable fixed point x_- after undergoing a rectangular overshoot,

$$r(t) = \begin{cases} R & \text{for } |t| < \dfrac{t_e}{2}, \\ -R_d & \text{for } |t| \geq \dfrac{t_e}{2}. \end{cases} \tag{2}$$

Consequently, for $|t| > t_e/2$, the dynamics has fixed points at

$$x_\pm = \frac{a\,R_d}{b} \pm \sqrt{\frac{R_d}{b}}\left[1 + \mathcal{O}\left(\frac{a^2\,R_d}{b}\right)\right]$$
$$\Rightarrow x_+ - x_- = 2\sqrt{\frac{R_d}{k_d}}, \tag{3}$$

with a coefficient k_d that takes the value of b_0 in the limit of $r \to 0$. Note that R_d is assumed to be small so that $\mathcal{O}\left(a^2 R_d/b\right)$ is negligible.

For $-t_e/2 \leq t \leq t_e/2$, the state $x(t)$ evolves according to the autonomous differential equation $\dot{x} = F(x;R)$ with initial condition

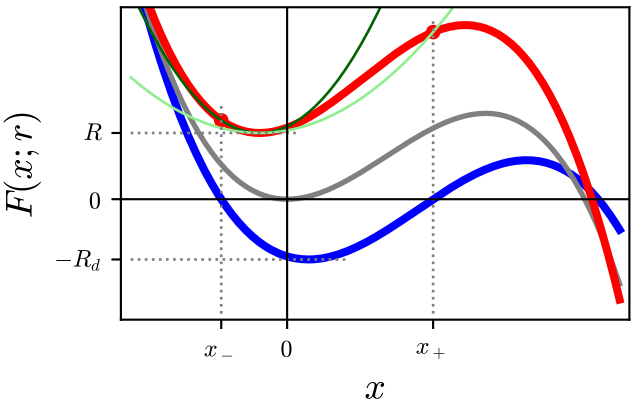

FIG. 2. The thick solid lines sketch the dynamics [Eq. (1)] for values $r = -R_d < 0$ (blue), $r = 0$ (gray), and $r = R > 0$ (red), respectively. The function $F(x; -R_d)$ takes negative values in the interval $(x_-; x_+)$ such that x_- and x_+ are a stable and an unstable fixed point, respectively. When r approaches zero, the width of the interval shrinks and the fixed points disappear in a saddle-node bifurcation at $r = 0$. The thin light and dark green lines provide a lower and an upper bound of $F(x, R)$ on $[x_-; x_+]$, respectively.

$x(-t_e/2) = x_-$. It will return to the initial state iff $x(t_e/2) < x_+$. Integration by separation of variables provides the following condition for the border t_B of stability, i.e., the maximum duration of the overshoot

$$t_B = \int_{x_-}^{x_+} \frac{\mathrm{d}x}{F(x;R)}. \tag{4}$$

Let $F(x;R)$ be continuous and bounded for $x \in [x_-; x_+]$, and let it take its minimum at the position $x_c \in [x_-; x_+]$ with a value $R_c = F(x_c, R)$. Then, there will be constant positive numbers $k_\pm$ such that for all $x \in [x_-; x_+]$, we have

$$R_c + k_- \, (x - x_c)^2 < F(x, R) < R_c + k_+ \, (x - x_c)^2.$$

In Fig. 2, these bounds are provided by a thin light green and dark green lines, respectively. The evaluation of the integral, Eq. (4), for the approximation where $F(x;R)$ is replaced by $R_c + k\,(x - x_c)^2$ is a continuous monotonic function of k. Moreover, k_+ and k_- provide lower and upper bounds of t_B. Therefore, there must be a value $k_c \in [k_-; k_+]$ such that

$$t_B = \int_{x_-}^{x_+} \frac{\mathrm{d}x}{R_c + k_c \, (x - x_c)^2}$$

$$= \frac{1}{\sqrt{k_c \, R_c}} \left[\operatorname{atan}\left(\sqrt{\frac{k_c}{R_c}} \, (x_+ - x_c) \right) - \operatorname{atan}\left(\sqrt{\frac{k_c}{R_c}} \, (x_- - x_c) \right) \right] \tag{5a}$$

$$\simeq \begin{cases} \dfrac{\pi}{\sqrt{k_c \, R_c}} & \text{for } \sqrt{\dfrac{k_c}{R_c}} \, |x_\pm - x_c| \gg 1, \\ \dfrac{x_+ - x_-}{R_c} & \text{for } \sqrt{\dfrac{k_c}{R_c}} \, (x_+ - x_-) \ll 1. \end{cases} \tag{5b}$$

In view of Eq. (3), we obtain the following prediction for the boundary of the stable domain:

$$T_B = \sqrt{k_d \, R_d} \;\; t_B = \begin{cases} \pi \sqrt{\dfrac{k_d}{k_c}} \; H^{-1/2} & \text{for } H = \dfrac{R_c}{R_d} \ll 1, \\ 2 \, H^{-1} & \text{for } H = \dfrac{R_c}{R_d} \gg 1. \end{cases} \tag{6}$$

Here, the dimensionless parameters

$$H = \frac{R}{R_d} \quad \text{and} \quad T = \sqrt{k_d \, R_d} \;\; t_e \tag{7}$$

characterize the strength and the duration of the overshoot.

The gray line in Fig. 1 shows the crossover, Eq. (6), for $k_d = k_c$. It features a crossover from a decay $T \simeq \pi \sqrt{k_d/k_c}/\sqrt{H}$ for small values of H, where the arcus tangens takes values close to $\pi/2$, to a decay $T \simeq 2/H$ for large values of H, where the arcus tangent approaches the identity. Such a shape of the boundary is observed whenever there are global bounds for k_d and k_c that apply for all considered values of R_d and the corresponding intervals $[x_-; x_+]$. We will further discuss this requirement in the Sec. V A.

Prior to elaborating on these conditions, we show that the crossover emerges also for a vast range of other temporal profiles of $r(t)$. Indeed, the crossover is observed for all parameter profiles where the order parameter decays to its asymptotic values faster than t^{-2}. This will be shown here for the dynamics

$$\dot{x} = k \, x^2 + r(t), \quad \text{with constant } \; k > 0 \tag{8}$$

that has been adopted to evaluate the integral Eq. (4). It allows us to determine the crossover of the stability boundary without superfluous technicalities.

Note that in this case $k_c = k_d = k$ and $x_+ = -x_- = \sqrt{R_d/k}$, and

$$T_B = \frac{2}{\sqrt{H}} \; \operatorname{atan} \frac{1}{\sqrt{H}}. \tag{9}$$

Equation (9) clearly shows how the crossover in T from an $H^{-1/2}$ decay to H^{-1} emerges due to the saturation of the atan-function. Moreover, it also suggests that the crossover may conveniently be studied in terms of the dimensionless variables,

$$c = T \sqrt{H} = \sqrt{kR} \, t_e \quad \text{and} \quad d = \frac{1}{\sqrt{H}} = \sqrt{\frac{R_d}{R}} \tag{10a}$$

such that Eq. (9) takes the form

$$c_R = \sqrt{kR} \, t_B = 2 \; \operatorname{atan}(d). \tag{10b}$$

III. BOUNDS FOR THE STABILITY BORDER

In order to derive bounds for the stability boundary, we compare the trajectories $x_1(t)$ and $x_2(t)$ for the overshoots $p_1(t)$ and $p_2(t)$. Their difference evolves as

$$\frac{\mathrm{d}}{\mathrm{d}t}(x_2 - x_1) = k \, (x_2 + x_1) \, (x_2 - x_1) + (p_2 - p_1). \tag{11}$$

For small values of $x_2 - x_1$, the solution of this equation takes the form of an exponential for $p_2 = p_1$, and its right-hand side is strictly positive for $p_2 > p_1$.

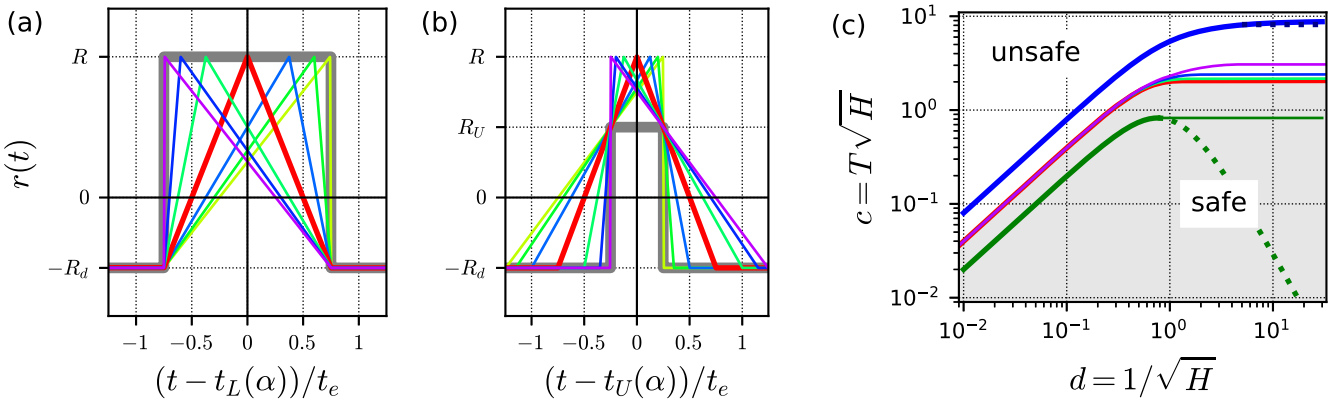

FIG. 3. Panels (a) and (b) show different triangular-shaped, i.e., piecewise-linear profiles $r(t)$, where α denotes the position of their respective maxima. They are all bounded from above (panel a) by a profile that takes the value R on an interval of duration $(1 + d^2)\, t_e$ and $-R_d$ outside the interval. They are all bounded from below (panel b) by a profile that takes the value R_U on an interval of duration $(1 - R_U/R)\, t_e$ and $-R_d$ outside the interval. The profiles in panels (a) and (b) are shifted by $t_L(\alpha)$ and $t_U(\alpha)$, respectively, in order to emphasize that α only induces a trivial time shift of the piecewise-constant bounds. According to Eqs. (12) and (14), these bounds provide the boundaries indicated by the uppermost solid (blue) line and the lowermost solid (green) line in panel (c), respectively. The thick green line (i.e., the lowermost curve) marks the result of Eq. (13) with $\Delta = 1 + d^2$. The thin green line indicates that for $d \gtrsim 1$, one can improve the lower bound by considering overshoots that do not reach down to $-R_d$, as in panel (a), but rather take a larger value $-R_d < -R_L < 0$. Thus, one establishes a lower bound that is provided by the lowest lying solid green line. There is also a (hardly visible) dotted black line that provides a slightly smaller upper bound for large values of d. The numerical values for the position of the stability boundary proceed mid-way between the bounds. They are marked by lines with colors matching those in the other two panels. Full details are provided in the main text.

Let the trajectories start at their respective stable fixed points. Then, $p_2 \geq p_1$ implies that $x_2 - x_1$ starts off positive semi-definite, and that x_2 becomes strictly larger than x_1 as soon as p_2 takes larger values than x_1. Combining this monotonicity condition with the result of Sec. II provides bounds for the position of the stability borders. For overshoots of triangular shape, this is demonstrated in Fig. 3.

A. Overshoots with finite support

We say that an overshoot has a finite support when there is a constant $\Delta > 1$, with

$$|t| > \Delta\, t_e \quad \Rightarrow \quad r(t) = -R_d.$$

An upper bound to the stability border is then provided by a rectangular overshoot where R_U takes the role of R such that the duration of the overshoot decreases by a factor of $\delta < 1$. Moreover, its amplitude is decreased by a factor of $R_U/R < 1$. With $T_U = \delta\, T$ and $H_U = (R_U/R)\, H$, and Eqs. (10a) and (9), one obtains an upper bound c_U for the stability boundary of overshoots with finite support,

$$c_U = \frac{c_R}{\delta\,\sqrt{R_U/R}} = \frac{2}{\delta\,\sqrt{R_U/R}}\,\operatorname{atan}\frac{d}{\sqrt{R_U/R}}. \tag{12}$$

The optimal, i.e., lowermost upper bound is obtained by taking into account the relation between δ and R_U and minimizing the right-hand side of Eq. (12) for different choices of δ in the range $0 < \delta < 1$.

For triangular-shaped overshoots, we have $\delta = 1 - R_U/R$ such that

$$c_U = \frac{2}{\delta\,\sqrt{1-\delta}}\,\operatorname{atan}\frac{d}{\sqrt{1-\delta}}. \tag{13}$$

For small values of d, the choice $\delta = 1/2$ is optimal, as one rapidly checks after introducing $\operatorname{atan}(d/\sqrt{1-\delta}) \simeq d/\sqrt{1-\delta}$. The solid blue line in Fig. 3(c) provides this boundary. For large d, one rather has $\operatorname{atan}(d/\sqrt{\Delta}) \simeq \pi/2$, and the value $\delta = 2/3$ provides a slightly smaller bound. It is provided by a dotted black line that is barely visible below the large d part of the solid blue line that shows Eq. (13).

A lower bound to the stability border is provided by the rectangular overshoot

$$r(t) = \begin{cases} -R_d & \text{for} \quad |t| > \Delta\, t_e, \\ R & \text{else.} \end{cases}$$

Hence, Eqs. (9) and (10) apply up to the substitution $t_e \to \Delta\, t_e$, i.e., with $d_L = d = \sqrt{R_d/R}$ and $c_L = \Delta\, c = \sqrt{kR}\,\Delta\, t_e$. Consequently, we obtain the following lower bound c_L for the stability boundary of overshoots with finite support,

$$c_L = \frac{c_R}{\Delta} = \frac{2}{\Delta}\,\operatorname{atan}(d). \tag{14}$$

For triangular-shaped overshoots, we have $\Delta = 1 + d^2$. The corresponding line is plotted as a thick green line in Fig. 3(c).

For small d, the lower bound provided by Eq. (14) provides a good idea about the boundary (solid thick green line). However, for $d \gtrsim 1$, it is rapidly decreasing while one would rather need a constant asymptotic value (dotted thick green line).

A better lower bound can obtained by adopting a rectangular overshoot profile with a lower value $0 > -R_L = -R\,(\Delta - 1) > -R_d$ with $1 < \Delta < 1 + d^2$. The smallest width that provides an

upper bound will then be $\Delta\ t_e$, and we obtain

$$c_L = \max_{\Delta>1} \frac{2}{\Delta} \operatorname{atan}\left(\sqrt{\Delta-1}\right) = \begin{cases} 0.8239\ldots & \text{for } d > \sqrt{\Delta_c - 1} \simeq 0.7654, \\ \dfrac{2}{1+d^2} \operatorname{atan}(d) & \text{else.} \end{cases} \tag{15}$$

This bound takes it maximum value for $\Delta_c \geq 1.5858$. This bound is provided by the horizontal thin green line in Fig. 3(c). For $d < \sqrt{\Delta_c - 1} \simeq 0.7654$, this value cannot be realized because the support of the overshoot has a width of $\Delta_{\max} = 1 + d^2$. Therefore, for $d < \sqrt{\Delta_c - 1}$, the optimal choice amounts to the width of the support, i.e., the expression provided by the thick solid green line in Fig. 3.

In Sec. III B, we extend our analysis to unimodal overshoots.

B. Bounds for unimodal overshoots

In Fig. 1, we announced that the exponent of the decay for large H is affected by a slow decay of $r(t)$ toward $-R_d$. In order to describe this dependence, we consider general overshoots of the unimodal form where $r(t)$ approaches $-R_d$ for $|t| \to \infty$, and it takes a maximum value of R. To simplify notations, we introduce the dimensionless time $\tau = 2t/t_e$, and we describe the overshoot by a function $R\,\rho(\tau)$ that provides the value of r when the width of $r(t)$ amounts to $\tau\ t_e/2$. For symmetric overshoots, this amounts to

$$\rho(\tau) = R^{-1}\, r\left(\frac{\tau\ t_e}{2}\right).$$

The notations are summarized in Fig. 4.

1. Lower bound

To derive a lower bound for unimodal overshoots, we consider rectangular overshoots that take a value of R for $|\tau| < \tau_L$ with $\tau_L > 1$, and the value $R\,\rho(\tau_L)$ otherwise. The green line in Fig. 4 provides the optimal case $\tau_L = \Delta$ and $\rho_L = -\rho(\Delta)$ that provides the maximum

$$c_L = \max_{\tau_L>1} \left[\frac{2}{\tau_L} \operatorname{atan}\sqrt{-\rho(\tau_L)}\right]. \tag{16}$$

The maximum is provided by the solution of

$$\sqrt{\rho_L}\ \operatorname{atan}\sqrt{\rho_L} = -\frac{\Delta}{2}\ \frac{\rho'(\Delta)}{1+\rho_L}. \tag{17}$$

For large d, we expect that the argument of the arcus tangent is large such that

$$-\frac{\Delta}{2}\ \frac{\rho'(\Delta)}{1+\rho_L} = \sqrt{\rho_L}\ \operatorname{atan}\sqrt{\rho_L} \simeq \frac{\pi}{2}\ \sqrt{\rho_L} - 1$$
$$\Rightarrow \sqrt{\rho_L} = \frac{2}{\pi}\left(1 - \frac{1}{2}\ \frac{\Delta\ \rho'(\Delta)}{1+\rho_L}\right) \quad \text{for} \quad \rho_L \gg 1. \tag{18a}$$

The bound $c_L^>$ is obtained by evaluating this expression for the given overshoot.

For small d, we expect that the argument of the arcus tangent in Eq. (17) is small such that

$$\rho_L = -\frac{1}{2}\ \Delta\ \rho'(\Delta) \quad \text{for} \quad \rho_L \ll 1. \tag{18b}$$

The bound $c_L^<$ is obtained by evaluating this expression for the given overshoot. Examples will be provided in Secs. IV B and IV A.

2. Upper bound

To derive an upper bound, we consider a rectangular overshoot that takes a value of $r = R\,\rho(\tau_U)$ for $|\tau| < \tau_U < 1$ and the value $r = -R_d$ otherwise. The blue line in Fig. 4 provides the optimal case $\tau_U = \delta$ and $\rho_U = \rho(\delta)$ that provides the minimum

$$c_U = \min_{0<\delta<1}\left[\frac{2}{\delta\ \sqrt{\rho_U}} \operatorname{atan}\frac{d}{\sqrt{\rho_U}}\right] \quad \text{with } \rho_U = \rho(\delta). \tag{19}$$

For large d, we expect that the argument of the arcus tangent is large. Approximating it by its asymptotic value $\pi/2$ and taking the derivative with respect to δ provides the condition

$$\rho_U = -\frac{1}{2}\ \delta\ \rho'(\delta) \quad \text{for } d \gg \sqrt{\rho}_U. \tag{20a}$$

The bound $c_U^>$ is obtained by evaluating this expression for the a given overshoot.

For small d, we expect that the argument of the arcus tangent is small. Approximating it to linear order and taking the derivative with respect to δ provides the condition

$$\rho_U = -\delta\ \rho'(\delta) \quad \text{for } d \ll \sqrt{\rho}_U. \tag{20b}$$

The bound $c_U^<$ is obtained by evaluating this expression for the a given overshoot.

The shape of the boundaries will depend on the form of the overshoot, $\rho(\tau)$. For the analysis, it is useful to observe that

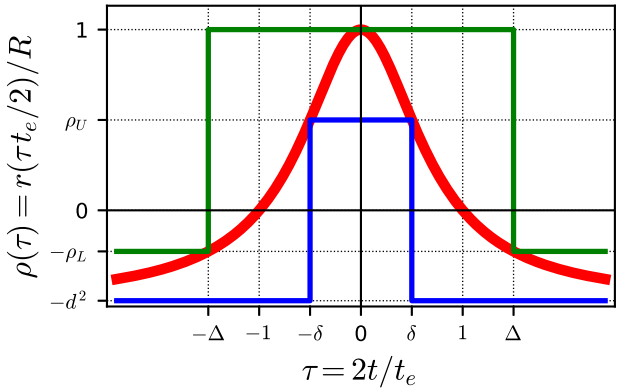

FIG. 4. Notations adopted to derive optimal bounds for general unimodal overshoots.

Eqs. (18b) and (20) take the form

$$\rho(\tau) = -f\,\tau\;\rho'(\tau), \tag{21}$$

with $f = -1/2$, $1/2$, and 1, respectively. Apart from the value of f, the cases only differ in the valid range of τ, and the limits to be taken when evaluating the arguments.

In the remainder of this section, we work out the limits for Gaussian overshoots and for overshoots with power-law tails.

IV. NONTRIVIAL EXAMPLES

A. Gaussian overshoots

Earlier literature[15] addressed Gaussian overshoots. In our notations, they take the form

$$\rho(\tau) = \frac{r(t)}{R} = d^2\;\left[-1 + \left(\frac{1+d^2}{d^2}\right)^{1-\tau^2}\right], \tag{22}$$

with derivative

$$\tau\;\rho'(\tau) = -2d^2\tau^2\;\ln\left(\frac{1+d^2}{d^2}\right)\left(\frac{1+d^2}{d^2}\right)^{1-\tau^2}.$$

For $d \gg 1$ and $d \gg \rho_L$, the expression (22) implies that

$$\rho_L = d^2\;\left[1 - \exp\left(\frac{1-\Delta^2}{d^2}\right)\right] = \Delta^2 - 1,$$
$$\Delta\;\rho'(\Delta) = -2\,\Delta^2$$

such that the implicit Eq. (18a) takes the form

$$\sqrt{\rho_L} = \frac{2}{\pi}\;\left(1 - \frac{1}{2}\;\frac{\Delta\;\rho'(\Delta)}{1+\rho_L}\right) = \frac{4}{\pi}.$$

Consequently, we obtain

$$c_L^{>} = \frac{2\,\mathrm{atan}\sqrt{\rho_L}}{\Delta} = \frac{2\,\mathrm{atan}\frac{4}{\pi}}{\sqrt{1+\left(\frac{4}{\pi}\right)^2}} \simeq 1.118, \tag{23}$$

as opposed to the numerically obtained value of 2.01. Indeed, in Fig. 5, there only is a small difference between the numerical data (solid red line) and the prediction Eq. (23) that is provided by a dashed blue line.

We inspect Eq. (21) to find the other bounds of the stability boundary. For the distribution Eq. (22), it takes the form

$$-1 + \frac{1+d^2}{d^2}\;\exp\left[-\tau^2\;\ln\left(\frac{1+d^2}{d^2}\right)\right]$$
$$= \frac{\rho(\tau)}{d^2} = -f\,\frac{\tau\;\rho'(\tau)}{d^2}$$
$$= 2f\tau^2\;\ln\left(\frac{1+d^2}{d^2}\right)\frac{1+d^2}{d^2}\exp\left[-\tau^2\ln\left(\frac{1+d^2}{d^2}\right)\right].$$

Introducing

$$X = \tau^2\;\ln\left(\frac{1+d^2}{d^2}\right) \tag{24a}$$

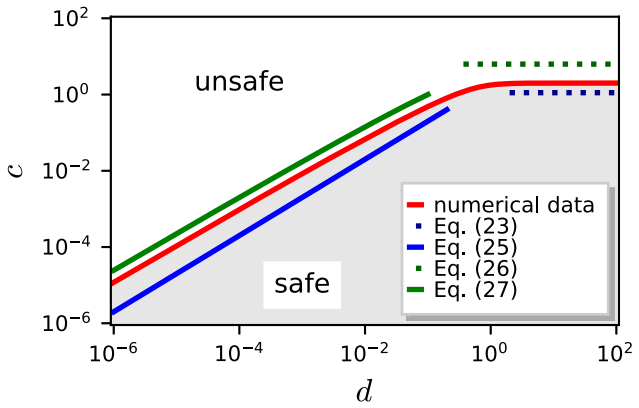

FIG. 5. The stability border for Gaussian overshoots, as defined in Eq. (22). The thick red line shows numerical data for the boundary. The other lines show upper and lower bounds for large and small values of d, respectively, as indicated in the legend.

allows us to write this condition in the compact form

$$\frac{d^2}{1+d^2} = (1 - 2fX)\;\mathrm{e}^{-X}. \tag{24b}$$

In order to evaluate the small d limit for the lower bound $c_L^{<}$, we evaluate Eq. (24) for $f = -1/2$. In this case, the first factor of the right-hand-side of Eq. (24b) is larger than one, and the product can only be small when X is large. The logarithm of Eq. (24b) provides

$$X = \ln\left(\frac{1+d^2}{d^2}\right) + \ln(1+X)$$
$$\simeq \ln\left(\frac{1+d^2}{d^2}\right) + \ln\left[1 + \ln\left(\frac{1+d^2}{d^2}\right)\right].$$

Based on Eq. (24a) with $\tau = \Delta$, we find

$$\Delta^2 = \frac{X}{\ln\left(\frac{1+d^2}{d^2}\right)} = 1 + \frac{\ln\left[1 + \ln\left(\frac{1+d^2}{d^2}\right)\right]}{\ln\left(\frac{1+d^2}{d^2}\right)},$$

and we obtain

$$\rho_L = -\rho(\Delta) = d^2\;\left[1 - \exp\left((1-\Delta^2)\;\ln\left(\frac{1+d^2}{d^2}\right)\right)\right]$$
$$= d^2\;\left[1 - \frac{1}{1+\ln\left(\frac{1+d^2}{d^2}\right)}\right] = \frac{d^2}{1+\frac{1}{\ln\left(\frac{1+d^2}{d^2}\right)}}.$$

We see that Δ is larger than one, and ρ_L is small. Consequently, $\mathrm{atan}(\sqrt{\rho_L}) \simeq \sqrt{\rho_L}$ and we find

$$c_L^{<} = \frac{2}{\Delta}\;\sqrt{\rho_L} \simeq 2\,d. \tag{25}$$

This bound is shown by the solid blue line in Fig. 5.

The large d limit for the upper bound is obtained by evaluating Eq. (24) for $f = 1/2$ and observing that $\ln(1 + d^{-2}) \simeq d^{-2}$. Therefore, $X \simeq (\delta/d)^2 \ll 1$ since $0 < \delta < 1$, Hence, Eq. (24b) reduces to

$$1 - \frac{1}{d^2} = \frac{d^2}{1+d^2} = (1 - X)\, \mathrm{e}^{-X} = 1 - 2\,\frac{\delta^2}{d^2}$$

such that

$$\delta^2 \simeq \frac{1}{2} \quad \text{and} \quad \rho_U = d^2 \left[-1 + \exp\left(\frac{1-\delta^2}{d^2}\right)\right] = \frac{1}{2}.$$

Consequently, we find that

$$c_U^{>} = \frac{2}{\delta\,\sqrt{\rho}_U}\ \mathrm{atan}\frac{d}{\sqrt{\rho}_U} = 2\pi. \tag{26}$$

This bound is shown by the dotted green line in Fig. 5.

Finally, the small d limit for the upper bound is obtained by evaluating Eq. (24) for $f = 1$. In this case, X cannot exceed the value of $1/2$ because the expression on the right-hand side of Eq. (24b) must be positive. Hence, the exponential cannot be small such that

$$X = \frac{1}{2} - d^2\,\sqrt{e} + \mathcal{O}(d^2).$$

In that case,

$$\left(\frac{1+d^2}{d^2}\right)^{-\delta^2} = \mathrm{e}^{-X} = \frac{1}{\sqrt{\mathrm{e}}}$$

and

$$\delta^2 = \frac{1}{2\ \ln\left(\frac{1+d^2}{d^2}\right)} \simeq \frac{1}{4\ |\ln d|}$$

such that

$$\rho_u = d^2\left(-1 + \frac{1+d^2}{d^2}\,\frac{1}{\sqrt{\mathrm{e}}}\right) \simeq \frac{1}{\sqrt{\mathrm{e}}}.$$

Consequently, we obtain

$$c_U^{<} = \frac{2\,d}{\delta\ \rho_U} = 4\,\sqrt{e}\ \ d\,\sqrt{|\ln d|}. \tag{27}$$

This bound is shown by the solid green line in Fig. 5. One clearly sees that the numerical data follow the $d\sqrt{|\ln d|}$ dependence provided by Eq. (27), rather than the linear dependence of Eq. (25). This suggests that the decay of the tails of the unimodal distribution might have an impact on the crossover from constant for large d to decaying for decreasing small d behavior. We will further explore that possibility by inspecting overshoots with power-law tails.

B. Overshoots with power-law tails

As an example of an overshoot with very broad, power-law tails, we inspect overshoots of the form

$$\rho(\tau) = d^2\ \ \frac{1 - |\tau|^\kappa}{d^2 + |\tau|^\kappa}, \tag{28a}$$

with derivative

$$\tau\ \rho'(\tau) = -d^2\ \frac{1+d^2}{\left(|\tau|^\kappa + d^2\right)^2}\ \kappa\ \ |\tau|^\kappa\,. \tag{28b}$$

For $\kappa = 2$, this amounts to a Cauchy distribution with baseline $-d^2$ (thick red line Fig. 4). The stability borders for $\kappa \in \{2, 3, 4\}$ are plotted in Fig. 1.

For $d \gg 1$, the implicit equation (18a) takes the form

$$\sqrt{\Delta^\kappa - 1} = \sqrt{\rho_L} = \frac{2}{\pi}\ \left(1 - \frac{1}{2}\ \frac{\Delta\ \rho'(\Delta)}{1+\rho_L}\right) = \frac{2}{\pi}\ \left(1 + \frac{\kappa}{2}\right).$$

This provides Δ, and, hence, the bound

$$c_L^{>} = \frac{\pi}{\Delta} = \frac{\pi}{\left(1 + \frac{4}{\pi^2}\ \left(1 + \frac{\kappa}{2}\right)^2\right)^{1/\kappa}}. \tag{29a}$$

Note that we dropped terms of order ρ_L^{-1} in the derivation of Eq. (18a). Hence, this expression holds at best when κ is not too small. Indeed, numerical data reveal that this approximation increases the prediction equation (29b) by about 70% for $\kappa = 2$ and still 20% for $\kappa = 10$. As a consequence, $c_L^{>}$ is not even a lower bound, but rather it is larger than the boundary for all $\kappa \geq 3$. However, it never exceeds the boundary by more than 2%, and the relative deviation decays like κ^{-1}. The solid green line in Fig. 6(a) demonstrates that it provides an excellent estimate of the asymptotic value of the border for large d. A proper lower bound can be found by numerically solving the large d approximation of the implicit equation (18a),

$$\sqrt{\rho}_L\ \mathrm{atan}\sqrt{\rho}_L = \frac{\kappa}{2}. \tag{29b}$$

The resulting expression is shown by the dotted line in Fig. 6(a).

We inspect Eq. (21) to find the other bounds of the stability boundary. For the distribution equation (28), it takes the form

$$\frac{1 - |\tau|^\kappa}{d^2 + |\tau|^\kappa} = \frac{\rho(\tau)}{d^2} = -\frac{f\,\tau\ \rho'(\tau)}{d^2} = \frac{1+d^2}{\left(\tau^\kappa + d^2\right)^2}\ \kappa\, f\, \tau^\kappa.$$

This provides a quadratic equation for τ^κ with solutions

$$\tau_\pm^\kappa = \frac{1}{2}\ \left[\left(1 - \kappa\, f\right) - \left(1 + \kappa\, f\right)\ d^2\right] \times \left[1 \pm \sqrt{1 + \frac{4\,d^2}{\left[\left(1 - \kappa\, f\right) - \left(1 + \kappa\, f\right)\ d^2\right]^2}}\right]. \tag{30}$$

In order to evaluate the small d limit for the lower bound $c_L^{<}$, we evaluate Eq. (30) for $f = -1/2$. For small d, the solution τ_-^κ has a

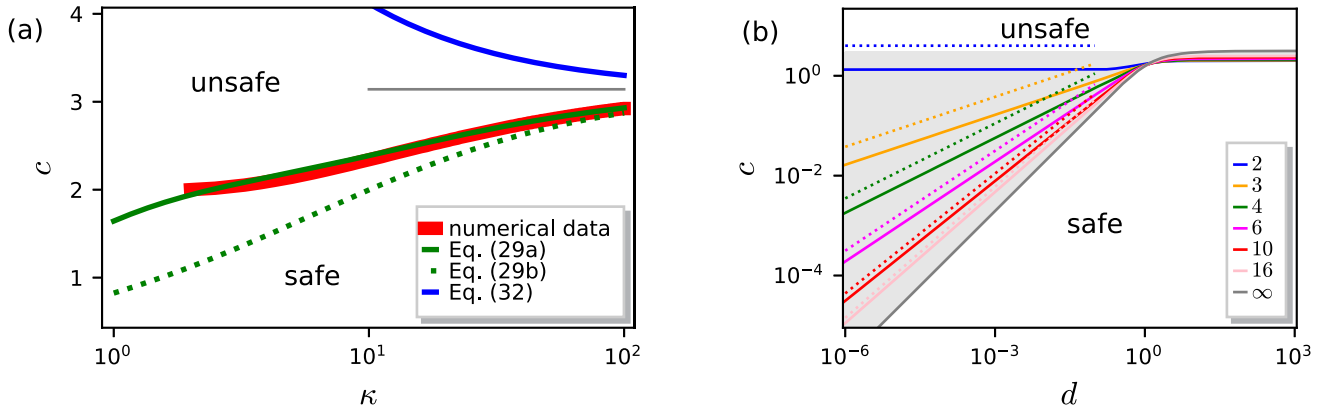

FIG. 6. Comparison of predictions and numerical data for the stability border for overshoots with power-law tail, as defined in Eq. (28). (a) The κ dependence of the position $c(d)$ of the stability boundary for $d = 100$. The red line provides numerical data for $\kappa > 2$. It amounts to the stability boundary between the safe and the unsafe region. The green lines are (approximations to the) lower bound $c_L^>$ discussed in the main text, the thin gray line provides the asymptotic value $\lim_{\kappa\to\infty} c(d) = \pi$, and the blue line is the upper bound $c_U^>$ [Eq. (32)]. (b) The thin solid lines show numerical results for the boundaries $c(d)$ with different κ, as provided in the figure legend, i.e., for $\kappa \in \{2, 3, 4, 6, 10, 16, \infty\}$ from top to bottom. The corresponding upper bounds for the decay for small d [Eq. (33)] are provided by dotted lines with matching colors. The κ dependence of the asymptotic value to the right is shown in panel (a).

negative sign, and it must be discarded. Consequently,

$$\Delta^\kappa = 1 + \frac{\kappa}{2} \quad \text{and} \quad \rho_L \simeq d^2\,\frac{\Delta^\kappa - 1}{\Delta^\kappa} = \frac{d^2\,\frac{\kappa}{2}}{1+\frac{\kappa}{2}},$$

and we find

$$c_L^< = \frac{2}{\Delta}\,\sqrt{\rho_L} = 2\,d\,\sqrt{\frac{\kappa}{2}}\,\left(1+\frac{\kappa}{2}\right)^{-\frac{1}{2}-\frac{1}{\kappa}}. \tag{31}$$

These lower bounds are linear functions that provide only a very rough lower bound. However, this bound can be improved noticeably by introducing another step in the piecewise-constant function adopted to derive the bound (see Fig. 7). We provide the according derivation in the Appendix.

For large d, the solution τ_+^κ has a negative sign, and it must be discarded. Moreover, the term added to one under the square root is now of order d^{-2}. Expanding the square root, one obtains

$$\delta^\kappa = \frac{1}{1+\frac{\kappa}{2}} \quad \text{and} \quad \rho_U \simeq 1 - \delta^\kappa = \frac{\frac{\kappa}{2}}{1+\frac{\kappa}{2}}.$$

In view of Eq. (19), we find

$$c_U^> = \frac{\pi}{\delta\,\sqrt{\rho_U}} = \frac{\pi}{\sqrt{\kappa/2}}\,\left(1+\frac{\kappa}{2}\right)^{\frac{1}{2}+\frac{1}{\kappa}}. \tag{32}$$

It is shown as a solid blue line in Fig. 6(a).

Finally, the small d limit for the upper bound is obtained by evaluating Eq. (30) for $f = 1$. For $\kappa > 1$, the solution τ_+^κ has a negative sign, and it must be discarded. Moreover, the term added to one under the square root is now of order d^2. Expanding the square root, one obtains

$$\delta^\kappa = \frac{d^2}{\kappa - 1} \quad \text{and} \quad \rho_U \simeq \frac{1}{1+\frac{1}{\kappa-1}} = \frac{\kappa-1}{\kappa},$$

and this provides

$$c_U^< = \frac{2\,d}{\delta\,\rho_U} = \frac{\kappa}{(\kappa-1)^{1-\frac{1}{\kappa}}}\,2\,d^{1-\frac{2}{\kappa}}. \tag{33}$$

These upper bounds are power laws in d with exponents $1 - 2/\kappa$. Figure 6(b) shows that this dependence is also observed in the numerical data. Moreover, for moderately large d the predicted prefactors approach those of the numerical data such that Eq. (33) provides an accurate estimate of the stability border.

In summary, we find that for large values of d the boundaries lie close to π. This behavior was also reported in earlier work.[15] However, for small values of d, the upper bound $c_U^<$ implies that the boundaries follow power laws with exponents $1 - 2/\kappa$. For $\kappa = 2$, there is no change. However, for $\kappa > 2$, the unsafe region is substantially increasing in this case, as shown in Fig. 6(b).

V. DISCUSSION

In the present section, we revisit the results reported in earlier literature, and we discuss the impact of our findings for applications.

A. Bounds for the general dynamics [Eq. (1)]

Let us now consider a time-dependent overshoot for the general dynamics [Eq. (1)]. As before, the asymptotic values of the control parameter are denoted as $R_d = \lim_{t\to\pm\infty} r(t)$. However, in this case, the maximum overshoot R will be defined by the implicit equation $R = \max_r \min_x F(x, r) = \min_x F(x, R) = F(x_c, R)$.

1. Lower bounds

Following the argumentation adopted in Sec. II, one shows that there is a value k_L such that

$$F(x, r) \le R + k_L\,(x - x_c)^2.$$

Consequently, there is a rectangular overshoot, as depicted by the green line in Fig. 4, that provides a lower bound for the stability border,

$$c_B = \sqrt{k_L\, R}\, t_B > c_L^+ + c_L^-,$$

with

$$c_L^\pm = \frac{1}{\Delta_\pm}\, \mathrm{atan}\left(\sqrt{\frac{k_L}{R}}\, \lambda_\pm\, |x_\pm - x_c|\right).$$

This expression is derived from Eq. (5a) by accounting for the increase of the left and right overshoot region by a factor of $\Delta_\pm$ and by a decrease in the distance of the fixed points from x_c by a factor $\lambda_\pm$. The increase in the length of the overshoot region is reflected by the condition $\Delta_+ + \Delta_- > 1$. The decrease in the distance between the fixed points from $x_+ - x_-$ to the $\tilde{x}_+ - \tilde{x}_-$ entails that $\tilde{x}_+ - \tilde{x}_- = \lambda_+ |x_+ - x_c| + \lambda_- |x_- - x_c| < x_+ - x_-$. The relation between the coefficients $\Delta_\pm$ and $\lambda_\pm$ is provided by the condition

$$\begin{aligned} 0 = F\big(\tilde{x}_\pm; R\, \rho(\pm\Delta_\pm)\big) &= R\, \rho(\pm\Delta_\pm) + k_L\, \big(\tilde{x}_\pm - \tilde{x}_c\big)^2 \\ &= R\, \rho(\pm\Delta_\pm) + k_L\, \lambda_\pm^2\, \big(x_\pm - x_c\big)^2, \end{aligned}$$

where $\tilde{x}_\pm$ are the positions of the fixed points for the parameter value $r = R\, \rho(\pm\Delta_\pm)$. Hence,

$$\begin{aligned} c_B &> \max_{\Delta_+ > 1} \frac{1}{\Delta_+}\, \mathrm{atan}\sqrt{-\rho(\Delta_+)} + \max_{\Delta_- > 1} \frac{1}{\Delta_-}\, \mathrm{atan}\sqrt{-\rho(-\Delta_-)} \\ &= \max_{\Delta > 1} \frac{2}{\Delta}\, \mathrm{atan}\sqrt{-\rho(\Delta)}. \end{aligned}$$

Hence, we recover our previous result [Eq. (16)]. The asymptotic power-law behavior of the upper bounds of the asymptotic stability boundaries of the general dynamics is faithfully described by the analysis of Eq. (8).

2. Upper bounds

Following the of argumentation adopted in Sec. II one shows that for every ρ_U there is a $k_U^*(\rho_U)$ such that

$$F(x, r) \geq R\, \rho_U + k_U(\rho_U)\, (x - x_c)^2.$$

In the following, we assume that $k_U = \inf_{0<\rho_U<1} k_U^*(\rho_U)$ takes a strictly positive value. (It is finite by construction.) Moreover, we introduce $k_\pm$ such that it describes the asymptotic fixed points,

$$0 = F(x_\pm; -R_d) = -R_d + k_\pm\, (x_\pm - x_c)^2.$$

Consequently, there is a rectangular overshoot, as depicted by the blue line in Fig. 4, that provides an upper bound for the stability border. In this case, Eq. (5a) provides

$$c_B = \sqrt{k_U\, R}\;\; t_B < c_U^+ + c_U^-,$$

with

$$c_U^\pm = \frac{1}{\delta_\pm\, \sqrt{\rho_U}}\, \mathrm{atan}\left(\sqrt{\frac{k_U}{k_\pm}}\, \frac{d}{\sqrt{\rho_U}}\right).$$

Here, $\rho_U = \rho(\pm\delta_\pm)$ such that

$$\begin{aligned} c_B < &\min_{0<\delta_+<1} \frac{1}{\delta_+\, \sqrt{\rho(\delta_+)}}\, \mathrm{atan}\left(\sqrt{\frac{k_U}{k_+}}\, \frac{d}{\sqrt{\rho(\delta_+)}}\right) \\ &+ \min_{0<\delta_-<1} \frac{1}{\delta_-\, \sqrt{\rho(-\delta_-)}}\, \mathrm{atan}\left(\sqrt{\frac{k_U}{k_-}}\, \frac{d}{\sqrt{\rho(-\delta_-)}}\right). \end{aligned} \tag{34}$$

In this expression, k_U and $k_\pm$ do not depend on δ_+ and δ_-. Hence, each summand is of the form of our previous condition Eq. (19), and the previous limits hold up to a substitution $d \to d\, \sqrt{k_U/k_\pm}$:

For large $d\, \sqrt{k_U/k_\pm}$, the bound approaches a constant. This will happen for large d whenever $\sqrt{k_U/k_\pm}$ does not decay like d^{-1} or faster.

For small $\sqrt{k_U/k_\pm}\, d$, the general dynamics obey the power laws derived for Eq. (8). Moreover, the ratio $k_U/k_\pm$ approaches a finite value for $d \to 0$ when k_U and $k_\pm$ are strictly positive and finite. Therefore, only the prefactor of the small-d asymptotics of the upper bounds may change. The exponents remain the same.

B. Earlier literature

Ritchie *et al.*[15] reported the following condition for the safe region:

$$d^b\, R\, t_e^2 \leq 16, \tag{35}$$

where d^b is the ratio of the square of decay rate λ to the stable fixed point and the position of the fixed point, $-x_c$, evaluated right at the bifurcation value,

$$\lambda = -\left.\frac{\mathrm{d}\dot{x}}{\mathrm{d}x}\right|_{x=-x_c} = 2k\, x_c = 2\, \sqrt{k\, |r|} \quad \Rightarrow \quad d^b = \lim_{r \nearrow 0} \frac{\lambda^2}{|r|} = 4\, k.$$

Hence, Eq. (35) is equivalent to

$$T = \sqrt{k R_d}\, t_e^2 \leq \sqrt{k R_d}\, \frac{4}{\sqrt{d^b\, R}} = \frac{2}{\sqrt{H}},$$

as provided by the uppermost, black dotted line in Fig. 1. Moreover, this also amounts to $c = T\, \sqrt{H} \leq 2$, which amounts to the horizontal, large d behavior observed in Figs. 3, 5, and 6.

The relation to our present work becomes transparent when adopting the dimensionless coordinates $\hat{x} = x/\sqrt{R_d/k}$ and $\tau = t/(T\, t_e)$ such that Eq. (8) takes the form

$$\frac{\mathrm{d}\hat{x}}{\mathrm{d}\tau} = \hat{x}^2 + H\, \frac{r(t)}{R}.$$

The derivation of Eq. (35) assumes that the forcing term is approximately parabolic in $[-t_e/2, t_e/2]$, and that the parameter forcing is of the form $\epsilon\, R_0 + r_h(\epsilon\, t)$ [cf. Eq. (2.2) and the discussion below Eq. (2.10) in Ritchie *et al.*[15]], where R_0 and $r_h(\epsilon\, t)$ take values of order one. The former condition implies that

$$H\, \frac{r(t)}{R} = H\, \left(1 - \left(\frac{2t}{t_e}\right)^2\right) = H - 4\, \left(\sqrt{H}\, \frac{\tau}{T}\right)^2,$$

and the latter condition stipulates that both H and $\sqrt{H}\,T$ take values of order $\epsilon \ll 1$. Hence,

$$T \lesssim \frac{\sqrt{H}}{\epsilon} \sim \frac{1}{\sqrt{H}}$$

is an immediate consequence of the adopted scaling.

The condition [Eq. (35)] was derived based on the condition that R is small and t_e is large. It does not involve the asymptotic values R_d. Here, we establish that the adopted scaling holds also for a general dynamics and for larger overshoots, where $H \gtrsim 1$, i.e., in particular, for $R \ll R_d$. Moreover, Ritchie *et al.*[15] assume that the control parameter takes a parabolic form beyond the threshold. The bounds provided in Sec. III establish that only minor changes of the numerical factor emerge in Eq. (35) when one drops this requirement. Moreover, the bounds also do not change when the overshoots are not symmetric in time with respect to the maximum [cf. Fig. 3 and the definition of $\rho(\tau)$ in Sec. III B].

C. Applications in earth system sciences

Figure 1 entails that the critical threshold H_c for short transgressions of duration T over the tipping point is substantially smaller than that previously expected: A previous work[15] suggested that $H_c \simeq 4/T^2$ while Eq. (10b) entails a crossover to linear scaling $c \sim d$ for small c and d. This implies that

$$H_c \sim \frac{1}{T} \ll \frac{4}{T^2}. \tag{36}$$

We provide two examples that indicated how this might be important in Earth system sciences.

The Earth climate system comprises subsystems that may exhibit threshold behavior.[19–21] These are the so-called climate tipping elements,[23,24] which can conceptually be represented through models that exhibit a saddle-node bifurcation (tipping point) such as the Amazon rainforest, the large ice sheets on Greenland and Antarctica, or the Atlantic Meridional Overturning Circulation.[25–30] The risk of at least temporarily transgressing such critical thresholds of the Earth system increases as global warming levels increase.[12,13] Indeed, it is unlikely that the Paris climate targets of limiting global warming to, at best, 1.5 °C by the end of this century can be satisfied without an overshoot.[31–33] This will put some climate tipping elements at risk of losing their stability[13] and may ultimately lead to severe biosphere degradation or large levels rises of sea level on the timescales of centuries and beyond. As compared to typical relaxation time scales of the climate system such an overshoot will be short, and according to Eq. (36), the maximum admissible trespassing H_c is substantially smaller than expected.

Shallow landslides and debris flow are triggered by intense and/or long-lasting rainfalls.[7–9] The stability threshold of slope stability has been described as a power law $I \sim D^{-\gamma}$, where I is the intensity of the rainfall and D is the duration, with exponents γ in the range between 0.4 (relatively undisturbed slopes at many different sites[7]) and 0.8 (humid-tropical environment in Puerto Rico[8]). A comprehensive recent overview of data is provided in Fig. 7 of Ref. 9. The present study suggests that it might be necessary to describe these data by a crossover between two power laws. Further work is needed to identify the appropriate nondimensionalized parameters. We expect that future data availability will enable better assessments of the risks of slope instabilities, in particular, when the frequency of extreme rainfall events increases with climate change (cf. Fig. 6 of Ref. 34).

VI. CONCLUSION

In this article, we discussed the boundary separating safe and unsafe overshoots when crossing a saddle-node bifurcation. For a piecewise-constant evolution of the control parameter, we established the asymptotic behavior of the stability boundary for small and large overshoots, Eq. (6), and we derived an analytical solution of the boundary [Eq. (9)] for a special case of the dynamics [Eq. (8)]. Based on a monotonicity condition [Eq. (11)], this result can be used to obtain rigorous upper and lower bounds of the boundary for different profiles of the control parameter. The conditions are formulated in terms of the dimensionless strength, H, and duration, T, of the overshoot—or equivalently in terms of $c = T\sqrt{H}$ and $d = 1/\sqrt{H}$, which turns out to be more convenient for the calculations. They apply for general unimodal shapes of the overshoot, i.e., also asymmetric profiles and when the overshoot does not have a quadratic maximum. Moreover, in Sec. V A, we explained why we respect them to apply also for general dynamics.

For small H, Ritchie *et al.*[15] established that the region of safe overshoots is bounded by a power law,

$$T < \frac{2}{\sqrt{H}} \quad \text{for} \quad H \lesssim 1.$$

Here, we extended this result by the following findings:

Ritchie *et al.*[15] assume that the control parameter takes a parabolic form beyond the threshold. We establish that, up to minor changes of the prefactor, the power law applies for $H \lesssim 1$, irrespective of the functional form of the time dependence of the order parameter. This is important since system changes might be driven by random fluctuations or abrupt policy changes, and the bounds established in the present paper provide bounds also for these cases.

Moreover, for $H \gtrsim 1$, there is a crossover to a different power law with an exponent that depends on the asymptotic decay of the control-parameter profile toward R_d. For control-parameter profiles with a finite support, we find that the safe region is bounded by a power law that decays much more rapidly,

$$T < \frac{c}{\sqrt{H}} \simeq \frac{2\phi}{H} \quad \text{for} \quad H \gtrsim 1, \text{ finite support},$$

where ϕ is a constant that depends on the shape of the profile [cf., Eqs. (12), (14), (10), and Fig. 3]. It takes values slightly larger than one.

For a Gaussian shape of the control parameter, the safe region is bounded by [cf. Eq. (27)]

$$T \lesssim \frac{4\sqrt{\mathrm{e}}\,\sqrt{|\ln d|}}{H} = 4\sqrt{2\mathrm{e}}\,\frac{\sqrt{\ln H}}{H} \quad \text{for} \quad H \gtrsim 1, \text{ Gaussian},$$

as shown in Figs. 1 and 5.

For a large-t asymptotics of $r(t) - R_d \sim t^{-\kappa}$, Eqs. (10) and (33) imply that

$$T \lesssim \frac{d^{1-\frac{2}{\kappa}}}{\sqrt{H}} = H^{-1+\frac{1}{\kappa}} \quad \text{for} \quad H \gtrsim 1, \text{ power law},$$

as shown in Figs. 1, 6, and 7.

Finally, our approach is not limited to control-parameter profiles, $r(t)$, that are symmetric with respect to the maximum. In Sec. III B, we explain how the bounds are constructed for arbitrary unimodal, i.e., also asymmetric, profiles (see also Fig. 3). Moreover, the nondimensionalization, which is adopted in the mathematical treatment of the equations, provides another remarkable insight into the nature of the boundary: Its shape is determined to a large extent by the dimensionless groups $H = R_d/R$ and the exceedance time $T = \sqrt{k\,R_d}\,t_e$. For the dynamics, Eq. (8), the boundary is invariant under changes in R_d, R, k, and t_e that preserve H and T. The shape of the tails matter for $H \gtrsim 1$, and a faster decay to the asymptotic state induces a crossover to power laws with faster decay (i.e., it decreases the safe region; cf. Fig. 1). In Secs. II and V A, we discussed how features of the dynamics far away from the threshold affect this assessment. For a general dynamics, the asymptotic exponents of the power laws will remain the same if the coefficients k_d and k_c in Eq. (6) and k_U, k_+, and k_- in Eq. (34) are bounded away from zero and infinity. Only the prefactors of the power laws and the shape of the crossover will then be affected.

We conclude that overshoots are less safe than previously thought. In particular, high and fast overshoots are more likely to trigger a tipping event (see Fig. 1). This emendation of the earlier literature is of pivotal importance when examining tipping risks in applications of nonlinear dynamics in finance, ecology, or climate.[4] For instance, in the field of climate tipping elements, assessing whether certain global warming overshoot trajectories can be considered safe or unsafe and which tipping risks are associated with them is key for avoiding potentially dangerous climate change pathways[35] (cf. Sec. V C). The present results provide the foundation to establish rigorous boundaries for the risks in different model scenarios.

ACKNOWLEDGMENTS

We are thankful for the fruitful discussions with Paul Ritchie, Jonathan F. Donges, and Vitus Benson. N.W. acknowledges support from the European Research Council Advanced Grant Project ERA (Earth Resilience in the Anthropocene, No. ERC-2016-ADG-743080). E.E. is grateful for support of the German Academic Scholarship Foundation and the funding through the Postgraduate Scholarship granted by the Free State of Saxony.

AUTHOR DECLARATIONS

Conflict of Interest

The authors have no conflicts to disclose.

Author Contributions

Elias Enache: Formal analysis (lead); Funding acquisition (lead); Methodology (equal); Writing – original draft (lead). **Oleksandr Kozak:** Formal analysis (equal); Methodology (equal); Validation (lead); Writing – original draft (supporting); Writing – review & editing (supporting). **Nico Wunderling:** Conceptualization (lead); Funding acquisition (equal); Methodology (supporting); Project administration (lead); Supervision (equal); Writing – original draft (equal); Writing – review & editing (equal). **Jürgen Vollmer:** Conceptualization (lead); Formal analysis (lead); Funding acquisition (supporting); Methodology (lead); Project administration (lead); Supervision (lead); Validation (supporting); Visualization (lead); Writing – original draft (equal); Writing – review & editing (lead).

DATA AVAILABILITY

The data that support the findings of this study are available from the corresponding author upon reasonable request.

APPENDIX: IMPROVED LOWER BOUND FOR OVERSHOOTS WITH POWER-LAW TAILS

Equation (31) provides a lower bound to the stability border, $c(d)$, which is a linear function of d, while the numerical data indicate that it scales like $d^{1-2/\kappa}$. We will demonstrate here how the bound can be improved by introducing another step in the piecewise-constant function adopted to derive the bound [see the green line in Fig. 7(a) as opposed to the one in Fig. 4].

In this case, the following expression still holds for $-\Delta < \tau \le -\delta$:

$$-\frac{t_e}{2} \le t \le \frac{t_e}{2}: \quad \frac{x(t)}{x_c} = \sqrt{\frac{R}{R_d}}\,\tan\left[\sqrt{kR}\left(t+\frac{t_e}{2}\right) - \operatorname{atan}\sqrt{\frac{R_d}{R}}\right] = \sqrt{H}\,\tan\left[T\sqrt{H}\left(\frac{t}{t_e}+\frac{1}{2}\right) - \operatorname{atan}\frac{1}{\sqrt{H}}\right].$$

We use the resulting value of $x(-\delta t_e/2)$ as initial condition for further integration. This provides

$$\frac{x(\tau\, t_e/2)}{x_c} = \sqrt{H}\,\tan\left(\frac{1}{2}\,T\sqrt{H}\,(\tau+\delta) + \arctan\left[\sqrt{\rho_U}\,\tan\left(T\sqrt{\rho_U H}\,\frac{\Delta-\delta}{2} - \arctan\sqrt{\frac{\rho_L}{\rho_U}}\right)\right]\right) \quad \text{for } -\delta \le \tau < \delta,$$

where $\rho_U = \rho(\delta)$ and $\rho_L = -\rho(\Delta)$.

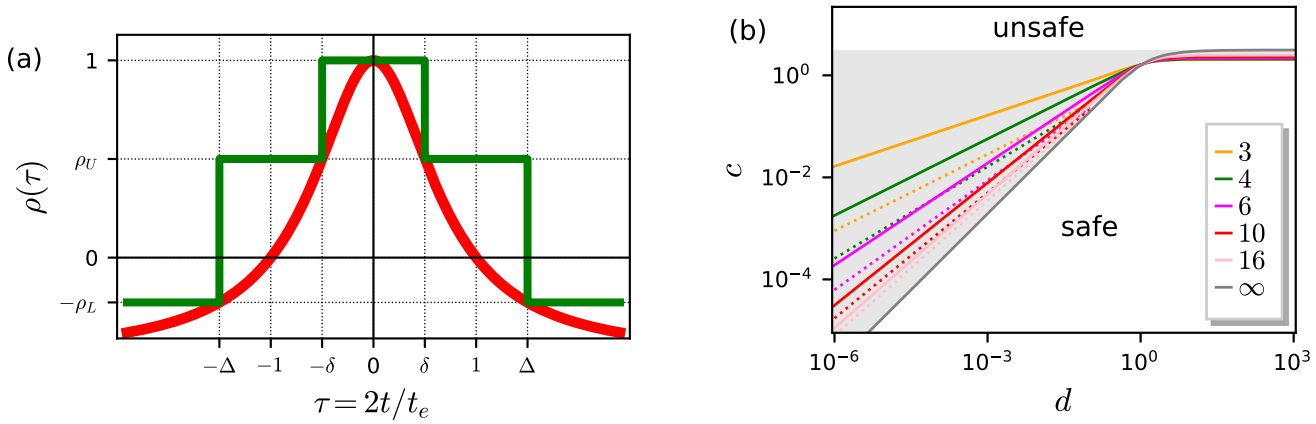

FIG. 7. Lower bound based on a two-step approximation for unimodal overshoots. (a) Notations adopted to parameterize the piecewise-constant function evaluated to derive the improved lower bound. (b) Analogous plot to Fig. 6(b), but now with the lower bounds provided by Eq. (A2). For large κ, the bound approaches $2d$, as we also observed earlier.

The stability boundary is provided by the trajectory that will approach the unstable fixed point for $\tau \to \infty$. By time-reversal symmetry, this trajectory proceeds through the origin such that $x(0) = 0$. Hence, we obtain

$$\tan\frac{\delta\, T\sqrt{H}}{2} = -\sqrt{\rho_U}\,\tan\left(T\sqrt{\rho_U H}\;\frac{\Delta-\delta}{2} - \arctan\sqrt{\frac{\rho_L}{\rho_U}}\right).$$

Introducing $c = T\sqrt{H}$ and $d = 1/\sqrt{H}$ provides the lower bound c_L as the smallest value of c that is a solution of the implicit equation

$$\tan\frac{c\,\delta}{2} = -\sqrt{\rho_U}\,\tan\left(c\sqrt{\rho_U}\;\frac{\Delta-\delta}{2} - \arctan\sqrt{\frac{\rho_L}{\rho_U}}\right).$$

Here, the minimization is performed by looking for the optimal choice of δ and Δ. The corresponding result for a single step was Eq. (16).

We will now evaluate this implicit equation for small values of c and $\rho(\tau)$ provided in Eq. (28). By definition, we have $0 < \delta < 1$ such that the argument of the tangent of the left-hand side of the equation is small, $c\,\delta/2 \ll 1$. To evaluate the right-hand side, we observe that $\tan(a-b) = (\tan a - \tan b)/(1+\tan a\,\tan b)$ and that also $c\sqrt{\rho_U}(\Delta-\delta) \ll 2$ will be small. This provides

$$\frac{c\,\delta}{2\sqrt{\rho_U}} = \frac{\sqrt{\frac{\rho_L}{\rho_U}} - c\sqrt{\rho_U}\;\frac{\Delta-\delta}{2}}{1+\sqrt{\frac{\rho_L}{\rho_U}}\;c\sqrt{\rho_U}\;\frac{\Delta-\delta}{2}}$$

$$\Rightarrow\; 0 = c^2\,\rho_L + 2\,c\sqrt{\rho_L}\left(\frac{\rho_U}{\delta} + \frac{1}{\Delta-\delta}\right) - \frac{4\,\rho_L}{\delta\,(\Delta-\delta)}$$

$$\Rightarrow\; c_L \simeq \max_{\delta,\Delta}\frac{2\sqrt{-\rho(\Delta)}}{\delta+\rho(\delta)\,(\Delta-\delta)}. \tag{A1}$$

The maximum will be taken for the value of δ that minimizes the denominator,

$$0 = \frac{\partial}{\partial\delta}\left[\delta+\rho(\delta)\,(\Delta-\delta)\right] = 1-\rho(\delta)+\left(\frac{\Delta}{\delta}-1\right)\,\delta\,\rho'(\delta).$$

We insert Eq. (28b), observe that $\Delta \gg \delta$, and keep only leading-order terms in d,

$$\delta^{\kappa+1} = \Delta\,\kappa\,d^2 \quad\text{and}\quad \rho_U = \rho(\delta) = \frac{\delta}{\Delta\,\kappa}.$$

Next, we evaluate the Δ-derivative of Eq. (A1),

$$0 = \frac{\partial}{\partial\Delta}\frac{2\sqrt{-\rho(\Delta)}}{\delta+\rho(\delta)\,(\Delta-\delta)}$$

$$\Rightarrow\; 2\,\rho(\Delta)\,\rho_U = \rho'(\Delta)\;\left(\delta\,(1-\rho_U)+\Delta\,\rho_U\right).$$

In view of $d^2 \ll 1 < \Delta$, this entails

$$\frac{\kappa}{\Delta^\kappa-1} \simeq \frac{\Delta\,\rho'(\Delta)}{\rho(\Delta)} = \frac{2\Delta\,\rho_U}{\delta\,(1-\rho_U)+\Delta\,\rho_U} = \frac{2}{\kappa+1-\frac{\delta}{\Delta}} \simeq \frac{2}{\kappa+1}$$

such that

$$\Delta^\kappa = 1+\frac{\kappa\,(1+\kappa)}{2}$$

and

$$\rho_L = d^2\,\frac{\Delta^\kappa-1}{\Delta^\kappa} = d^2\,\frac{\kappa\,(1+\kappa)}{2+\kappa\,(1+\kappa)}.$$

Inserting these expressions into c_L provides

$$c_L^< \simeq \frac{2\sqrt{\rho_L}}{\delta+\Delta\,\rho_U}$$

$$= d^{1-\frac{2}{1+\kappa}}\,\sqrt{\frac{2\,\kappa}{1+\kappa}}\;\kappa^{1-\frac{1}{1+\kappa}}\;\left(1+\frac{\kappa\,(1+\kappa)}{2}\right)^{-\frac{1}{2}-\frac{1}{\kappa\,(1+\kappa)}}. \tag{A2}$$

In Fig. 7(b), these bounds are compared to the numerical results. The present two-step approach improves the lower bound from a linear function for all values of κ [Eq. (31)] to become a power-law

in d with an exponent $1 - 2/(1 + \kappa)$. This exponent is much closer to $1 - 2/\kappa$, as observed in the numerical data and the upper bound [Eq. (33)] and—in principle—it can further be improved by introducing still another step in the piecewise-constant function adopted to calculate the bound.

REFERENCES

[1]W. Horsthemke and R. Lefever, *Noise-Induced Transitions in Physics, Chemistry, and Biology* (Springer-Verlag, New York, 1984).
[2]M. Scheffer, J. Bascompte, W. A. Brock, V. Brovkin, S. R. Carpenter, V. Dakos, H. Held, E. H. Van Nes, M. Rietkerk, and G. Sugihara, "Early-warning signals for critical transitions," Nature **461**, 53–59 (2009).
[3]T. M. Lenton, "Environmental tipping points," Annu. Rev. Environ. Resour. **38**, 1–29 (2013).
[4]C. D. Brummitt, G. Barnett, and R. M. D'Souza, "Coupled catastrophes: Sudden shifts cascade and hop among interdependent systems," J. R. Soc. Interface **12**, 20150712 (2015).
[5]U. Feudel, A. N. Pisarchik, and K. Showalter, "Multistability and tipping: From mathematics and physics to climate and brain—Minireview and preface to the focus issue," Chaos **28**, 033501 (2018).
[6]G. Datseris, K. Luiz Rossi, and A. Wagemakers, "Framework for global stability analysis of dynamical systems," Chaos **33**, 073151 (2023).
[7]N. Caine, "The rainfall intensity-duration control of shallow landslides and debris flows," Geogr. Ann. Ser. A: Phys. Geogr. **62**, 23–27 (1980).
[8]M. C. Larsen and A. Simon, "A rainfall intensity-duration threshold for landslides in a humid-tropical environment, Puerto Rico," Geogr. Ann. Ser. A: Phys. Geogr. **75**, 13–23 (1993).
[9]B.-G. Chae, H.-J. Park, F. Catani, A. Simoni, and M. Berti, "Landslide prediction, monitoring and early warning: A concise review of state-of-the-art," Geosci. J. **21**, 1033–1070 (2017).
[10]R. M. May, S. A. Levin, and G. Sugihara, "Ecology for bankers," Nature **451**, 893–894 (2008).
[11]T. Gross, "Not one, but many critical states: A dynamical systems perspective," Front. Neural Circuits **15**, 614268 (2021).
[12]P. D. Ritchie, J. J. Clarke, P. M. Cox, and C. Huntingford, "Overshooting tipping point thresholds in a changing climate," Nature **592**, 517–523 (2021).
[13]N. Wunderling, R. Winkelmann, J. Rockström, S. Loriani, D. I. Armstrong McKay, P. D. Ritchie, B. Sakschewski, and J. F. Donges, "Global warming overshoots increase risks of climate tipping cascades in a network model," Nat. Clim. Change **13**, 75–82 (2023).
[14]T. Möller, A. E. Högner, C.-F. Schleussner, S. Bien, N. H. Kitzmann, R. D. Lamboll, J. Rogelj, J. F. Donges, J. Rockström, and N. Wunderling, "Achieving net zero greenhouse gas emissions critical to limit climate tipping risks," Nat. Commun. **15**, 6192 (2024).
[15]P. Ritchie, Ö. Karabacak, and J. Sieber, "Inverse-square law between time and amplitude for crossing tipping thresholds," Proc. R. Soc. A **475**, 20180504 (2019).
[16]C. Kuehn, "A mathematical framework for critical transitions: Bifurcations, fast–slow systems and stochastic dynamics," Physica D **240**, 1020–1035 (2011).
[17]P. Ashwin, S. Wieczorek, R. Vitolo, and P. Cox, "Tipping points in open systems: Bifurcation, noise-induced and rate-dependent examples in the climate system," Philos. Trans. R. Soc. A: Math. Phys. Eng. Sci. **370**, 1166–1184 (2012).
[18]J. C. Rocha, G. Peterson, Ö. Bodin, and S. Levin, "Cascading regime shifts within and across scales," Science **362**, 1379–1383 (2018).
[19]L. Drouet, V. Bosetti, S. A. Padoan, L. Aleluia Reis, C. Bertram, F. Dalla Longa, J. Després, J. Emmerling, F. Fosse, K. Fragkiadakis *et al.*, "Net zero-emission pathways reduce the physical and economic risks of climate change," Nat. Clim. Change **11**, 1070–1076 (2021).
[20]K. Riahi, C. Bertram, D. Huppmann, J. Rogelj, V. Bosetti, A.-M. Cabardos, A. Deppermann, L. Drouet, S. Frank, O. Fricko *et al.*, "Cost and attainability of meeting stringent climate targets without overshoot," Nat. Clim. Change **11**, 1063–1069 (2021).
[21]J. Rogelj, D. Huppmann, V. Krey, K. Riahi, L. Clarke, M. Gidden, Z. Nicholls, and M. Meinshausen, "A new scenario logic for the Paris agreement long-term temperature goal," Nature **573**, 357–363 (2019).
[22]C. M. Bender and S. A. Orszag, *Advanced Mathematical Methods for Scientists and Engineers* (Springer Science & Business Media, Singapore, 1987).
[23]T. M. Lenton, H. Held, E. Kriegler, J. W. Hall, W. Lucht, S. Rahmstorf, and H. J. Schellnhuber, "Tipping elements in the Earth's climate system," Proc. Natl. Acad. Sci. U.S.A. **105**, 1786–1793 (2008).
[24]D. I. Armstrong McKay, A. Staal, J. F. Abrams, R. Winkelmann, B. Sakschewski, S. Loriani, I. Fetzer, S. E. Cornell, J. Rockström, and T. M. Lenton, "Exceeding 1.5 °C global warming could trigger multiple climate tipping points," Science **377**, eabn7950 (2022).
[25]A. Staal, S. C. Dekker, M. Hirota, and E. H. van Nes, "Synergistic effects of drought and deforestation on the resilience of the south-eastern Amazon rainforest," Ecol. Complex. **22**, 65–75 (2015).
[26]A. Levermann and R. Winkelmann, "A simple equation for the melt elevation feedback of ice sheets," Cryosphere **10**, 1799–1807 (2016).
[27]H. Stommel, "Thermohaline convection with two stable regimes of flow," Tellus **13**, 224–230 (1961).
[28]P. Cessi, "A simple box model of stochastically forced thermohaline flow," J. Phys. Oceanogr. **24**, 1911–1920 (1994).
[29]N. Wunderling, J. Krönke, V. Wohlfarth, J. Kohler, J. Heitzig, A. Staal, S. Willner, R. Winkelmann, and J. F. Donges, "Modelling nonlinear dynamics of interacting tipping elements on complex networks: The PyCascades package," Eur. Phys. J. Spec. Top. **230**, 3163–3176 (2021).
[30]J. Kohler, N. Wunderling, J. F. Donges, and J. Vollmer, "Complex networks of interacting stochastic tipping elements: Cooperativity of phase separation in the large-system limit," Phys. Rev. E **104**, 044301 (2021).
[31]V. Masson-Delmotte, P. Zhai, H.-O. Pörtner, D. Roberts, J. Skea, P. R. Shukla, A. Pirani, W. Moufouma-Okia, C. Péan, R. Pidcock *et al.*, "*An IPCC Special Report on the Impacts of Global Warming of Global Warming of 1.5* °C (Cambridge University Press, 2018), Vol. 1, pp. 93–174.
[32]C.-F. Schleussner, G. Ganti, J. Rogelj, and M. J. Gidden, "An emission pathway classification reflecting the Paris agreement climate objectives," Commun. Earth Environ. **3**, 135 (2022).
[33]J. Rogelj, T. Fransen, M. G. den Elzen, R. D. Lamboll, C. Schumer, T. Kuramochi, F. Hans, S. Mooldijk, and J. Portugal-Pereira, "Credibility gap in net-zero climate targets leaves world at high risk," Science **380**, 1014–1016 (2023).
[34]V. Masson-Delmotte, P. Zhai, A. Pirani, S. L. Connors, C. Péan, S. Berger, N. Caud, Y. Chen, L. Goldfarb, M. Gomis *et al.*, "Climate change 2021: The physical science basis," in *Contribution of Working Group I to the Sixth Assessment Report of the Intergovernmental Panel on Climate Change* (Cambridge University Press, Cambridge, UK, 2021), Vol. 2, p. 2391.
[35]L. Kemp, C. Xu, J. Depledge, K. L. Ebi, G. Gibbins, T. A. Kohler, J. Rockström, M. Scheffer, H. J. Schellnhuber, W. Steffen *et al.*, "Climate endgame: Exploring catastrophic climate change scenarios," Proc. Natl. Acad. Sci. U.S.A. **119**, e2108146119 (2022).